CHAPTER X UCM/MMP COOKOFF MODELS FOR EXPLOSIVES CONTAINING RDX

Michael L. Hobbs[a*], Michael J. Kaneshige[a], William W. Erikson[a]

[a]Sandia National Laboratories, Albuquerque NM USA

*corresponding author, mlhobbs@sandia.gov

X ABSTRACT

Determining the thermal response of energetic materials containing RDX (hexahydro-1,3,5-tri-nitro-1,3,5-triazine) is difficult due to pressure dependent reactions that occur within the interior of explosives along with the various binders that decompose simultaneously with the RDX. Recently, we have developed a Universal Cookoff Model (UCM) coupled to a MicroMechanics Pressurization (MMP) model to account for pressure-dependent reactions occurring on the interior of explosives. We assume that the decomposition gases accumulate in uniformly distributed defects that grow spherically until local damage causes the closed pressurizing pore to become open. As the explosive is damaged, the gases can move to other open pores or even into the surrounding headspace. One drawback of the combined UCM/MMP model is insufficient parameters for our RDX based explosives. Here, we use historic data from the Sandia Instrumented Thermal Ignition (SITI) experiment to create UCM/MMP models for seven RDX containing explosives: 1) **Comp-B3** (60 wt% RDX and 40 wt% 2,4,6-trinitrotoluene or TNT), 2) **Comp-C4** (91 wt% RDX, 5.3 wt% dioctyl adipate or DOA, 2.1 wt% polyisobutylene, and 1.6 wt% oil, 3) **PBX 9407** (94 wt% RDX and 6% vinyl chloride/chlorotrifluoro ethylene copolymer or VCTFE, 4) **PBXN-109** (64 wt% RDX 20% Aluminum, 8% hydroxyl-terminated polybutadiene or HTPB, and 8% DOA), 5) **RDX** (assumed

pure), 6) **Semtex 1H** (43 wt% RDX, 43 wt% PETN, 2.5 wt% polyethylene and 11.6 wt% dioctyl sebacate), and 7) **XTX-8004** (80 wt% RDX and 20 wt% Sylgard^{TM}). The models are validated with data from other laboratories.

X.1 Universal cookoff model/micromechanics pressurization (UCM/MMP)

X.1.1 *Energy equation*. Predicting thermal ignition requires solving the conductive energy equation,

$$\rho C_p \frac{\partial T}{\partial t} = \nabla \cdot (k \nabla T) + r_x h_r + \dot{q}_{melt} \quad (1)$$

by including volumetric sources for decomposition ($r_x h_r$) and latent energy sinks ($\dot{q}_{melt}$). The momentum equation can also be solved for flow if the explosive melts (e.g., Comp-B3, TNT, PETN, etc). From previous work [1], we have found that flow effects are hindered by non-melting constituents such as RDX in Comp-B3 that cause the material to stay largely in place. For such situations, flow effects can adequately be accounted for by increasing the thermal conductivity (k) at the melting point. Specific heats (C_p), thermal conductivities (k), and rate coefficients (n, m, E, σ, and λ_m) in Eq. (1) can be determined from experiments coupled with finite element simulations [2]. Parameters for RDX containing explosives are given in Tables X.1 and X.2.

Initially, the universal cookoff model [3] was developed to provide a simple framework for describing thermal ignition of energetic materials. This framework consisted of a single desorption reaction for moisture, two explosive reactions with one being gas-phase dominated and the other being condensed-phase dominated, and a binder reaction. The success of this model is attributed to the flexible form of the distributed rate expressions.

Table X.1 *Thermophysical Properties*[a].

Name	T, K	C_p, J/kgK	T, K	k, W/mK (ρ_b, kg/m^3)
Comp-B3	300	1084	300	0.2 (1710)
	350	1240	440	0.2 (1710)
	477	1680	477	0.8[b] (1710)
Comp-C4	300	1004	300	0.16 (1500)
	600	1818	600	0.16 (1500)
PBX 9407	273	1008	400	0.20 (1625)
	482	1681	478	0.20 (1625)
PBXN-109	300	1500	300	0.4 (1650)
	600	1500	600	0.4 (1650)
RDX	300	1004	300	0.20 (1650)
	623	1760	600	0.20 (1650)
Semtex1H	300	1145	300	0.18 (1530)
	400	1470	500	0.24 (1530)
XTX-8004	298	1100	300	0.2 (1550)
	460	1520	600	0.2 (1550)

[a]Temperature dependent properties are interpolated linearly with constant extrapolation.
[b]Thermal conductivity (k) for Comp-B3 at 477 K was increased artificially from 0.3 to 0.8 W/mK to account for flow. If a true flow model is used, then k at 477 K is 0.3 W/mK.

Table X.2 *Kinetic parameters.*

Name	n	m	E, K	σ, K	RDX: λ_m	PETN: λ_m
Comp-B3	0.35	1.5	24500	-500	2	--
Comp-C4	0.16	2	25063	-1000	2	--
PBX 9407	0.23	0.5	22560	-400	10	--
PBXN-109	0.295	-1	18012	-400	2	--
RDX	0.295	3	29772	-400	4	--
Semtex1H	0[a]	-0.5	17200	-500	1	4[b]
XTX-8004	0.15	3	28020	-1000	1	--

[a]No pressure measurements were available to determine n.
[b]Only PETN melt acceleration (λ_m = 4) was used in the Semtex1H model.

Distributed rates can be tuned to represent reaction forms ranging from diffusion-limited reactions (deceleratory) to auto-catalytic reactions (acceleratory).

Two drawbacks of the UCM framework are 1) the difficulty and variability of measuring small amounts of adsorbed moisture and 2) the separation of the explosive reactions from the binder reactions when decomposition products interact. In the current work, we eliminate the moisture desorption step and combined the two explosive reactions with the binder reaction to simplify the UCM framework. This simplified UCM framework is composed of a single first order reactions with respect to the explosive concentration [X]. The rate of explosive decomposition (r_x) is given by Eq. [2] with parameters provided in Table X.2.

$$r_x = 1.586 \times 10^{15} \left(\frac{P}{P_o}\right)^n \lambda T^m \exp\left[-\frac{(E+\xi\sigma)}{T}\right] [\mathrm{X}] \qquad (2)$$

X1.2 *Distributed Activation Energy.* In Eq. (2), the inverse of the standard normal distribution (ξ) is used to make the reactions self-accelerating or autocatalytic. The positive sign following the normalized activation energy (E in Eq. 2) causes the activation energy to decrease with the extent of reaction resulting in rate acceleration (for a negative value of σ). Figure X.1 shows the inverse of the standard normal distribution calculated with the Microsoft Excel function "ξ = NORM.INV(X/X$_o$,0,1)".

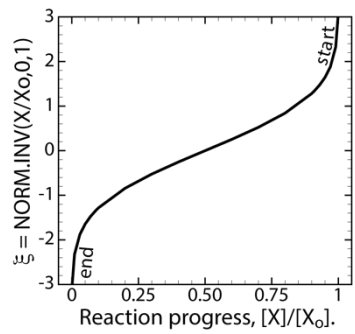

Figure X.1 Inverse of the standard normal distribution.

X.1.3 *Phase Change.* Most materials that decompose do not melt at a clearly defined temperature but melt over a temperature range referred to as the melty mush zone which begins at the solidus temperature (T_S) and ends at the liquidus temperature (T_L). The model includes RDX melting as well as TNT melting in Comp-B3 and PETN melting in Semtex 1H. Latent enthalpy is accounted for by increasing the specific heat within the phase change temperature range using an effective capacitance method.

The effective capacitance method is shown in Eq. (3) where the latent energy is released in a melty mush zone between the solidus temperature (Ts) and the liquidus temperature (T_L) using a Gaussian distribution. In this method, the specific heat is increased artificially within the mush zone to account for both caloric and latent contributions to the transient heat conduction term in the energy equation.

$$C_{eff} = C_p + \frac{\omega h_l}{\sigma\sqrt{2\pi}} e^{-\frac{z^2}{2}} \text{ with } \sigma = \frac{(T_m - T_S)}{3},\ T_m = \frac{(T_L + T_S)}{2},\ \text{and } z = \frac{(T - T_m)}{\sigma} \quad (3)$$

The effective capacitance method is used for constituents that melt in each of the explosive formulations. In Eq. (3), ω represents the mass fraction of the component that is melting, e.g., ω_{RDX}, ω_{TNT}, or ω_{PETN}, as shown in Table X.3. The solidus and liquidus temperature pairs that define the mush melt zone for RDX, TNT, and PETN as well as the latent melting enthalpies (h_l) for pure RDX, TNT, and PETN are also given in Table X.3. Other latent effects such as dissolution of RDX in molten TNT [4] or the α-PETN to β-PETN polymorphic phase change [5] are small when compared to melting and are neglected in the current work.

Table X.3 *Mass fractions of the melting components.*

Name	Mush Melt: 471-477 K h_l: 160000 J/kg ω_{RDX}	350-360 K 98450 J/kg ω_{TNT}	413-415 K 177000 J/kg ω_{PETN}
Comp-B3	0.60	0.40	0
Comp-C4	0.91	0	0
PBX 9407	0.94	0	0
PBXN-109	0.64	0	0
RDX	1.00	0	0
Semtex1H	0.43	0	0.43
XTX-8004	0.80	0	0

X1.3 *Phase change induced rate acceleration*. Rate acceleration caused by melting is usually significant when the boundary temperature exceeds the melting point of RDX or any other melting component. This acceleration is modelled using a rate multiplier, λ, which is 1 at the solidus temperature (T_s) and λ_m at the liquidus temperature (T_L). The multiplier, λ_m, is given in Table X.2. The cosine ramp function in Eq. (4) was used to transition between these two temperatures for RDX:

$$\lambda = \begin{cases} 1, & T \le T_S \\ 1 + 0.5\left(1 - [\lambda_m - 1]\cos\left[\pi\frac{(T - T_S)}{(T_S - T_L)}\right]\right) & T_S < T < T_L \\ \lambda_m & T \ge T_L \end{cases} \quad (4)$$

X.1.4 *Explosive decomposition*. The initial explosive compositions are given in Table X.4. Other properties in this table show differences in the various RDX formulations, including the molecular formula, the explosive's molecular

weight (Mw_x), the oxygen balance (O_2 bal.) assuming C forms CO_2 and H forms H_2O, the theoretical maximum density (TMD, ρ_{co}), the heat of formation (h_f), the detonation velocity (D) determined at TMD, and the low-pressure adiabatic flame temperature (T_a). The detonation velocities and adiabatic flame temperatures were predicted with the JCZ3 equation of state (EOS) using the TIGER code with the JCZS3 thermodynamic database [6].

TIGER was also used to predict the equilibrium product hierarchy shown in Table X.5 for each of the explosives at 400 K and 1 bar. This thermodynamic state is representative of typical cookoff conditions and doesn't change much, even at elevated pressures. A simplified reaction scheme is also given in Table X.4 showing formation of a single gas and various condensed species:

$$X \rightarrow \alpha G + \beta Al + \gamma C + \delta SiO_2 \ . \qquad (5)$$

The explosive concentration [X] can be determined with $\frac{dX}{dt} = -r_x$ with $[X]_o = \omega_x \rho_{bo}/Mw_x$. In Eq. (5), X represents the explosive. G, Al, C, and SiO_2 represent decomposition gases, aluminum, carbon, and silicon dioxide, respectively. The stoichiometric coefficients (α, β, γ, and δ) are given in Table 5. For example, when X = Comp-B3, α = 6.81, β = 0, γ = 2.72. and δ = 0.

Table X.4 *Explosives containing RDX.*

Name	Comp. (wt.%), formula	Mw_x g/mol	O_2 bal.	ρ_{co}, kg/m^3	h_f kJ/mol	D^b km/s	T_a K
Comp-B3	RDX/TNT (60/40) $C_{4.58}H_{5.6}N_{4.82}O_6$	224.2	-42.6	1742	16.9	7.81	2651
Comp-C4	RDX/DOA/PIB/Oil 91/5.3/2.1/1.6 $C_{3.83}H_{7.5}N_{5.2}O_{5.23}$	211.5	-46.1	1659	16.8	7.90	2471
PBX 9407	RDX/VCTFE (94/6) $C_{3.1}H_{5.9}N_{5.6}O_{5.6}Cl_{0.18}F_{0.18}$	221.8	-24.2	1799	18.4	8.37	2880
PBXN-109	RDX/AL/HTPB/DOA 64/20/8/8 $C_{1.61}H_{2.94}N_{1.44}O_{1.51}AL_{0.62}$	83.4	-78.7	1656	-4.7	7.24[c]	2033
RDX	RDX (100) $C_3H_6N_6O_6$	222.1	-21.6	1806	69	8.78	2930
Semtex 1H	RDX/PETN/Binder/Plastici. 65.5(max)/25(min)/2.5/11.6 or 43/43/2.5/11.5 $C_{4.8}H_{8.86}N_{3.8}O_{6.51}$	224.0	-53.7	1581	-226	7.45	2164
XTX	RDX/Sylgard™ 182 (80/20) $C_{2.57}H_6N_{3.44}O_{3.86}Si_{0.43}$	158.9	-51.8	1579	-176	7.72	2260

Table X.5 *Reaction hierarchy for pre-ignition reactions*

Name	Equilibrium reactions, heats for formation (h_f), and reaction enthalpies (h_{rxn})
Comp-B3	$C_{4.58}H_{5.6}N_{4.82}O_6 \rightarrow 2.54\ H_2O + 2.41\ N_2 + 1.73\ CO_2 + 0.13\ CH_4 + 2.72\ C$ Comp-B3 $\rightarrow$ 6.81 G + 2.72 C Mw_G = 28.1 g/mol; $h_{f,G}$ = -191.5 kJ/mol $h_{f,Comp\text{-}B3}$ = 16.9 kJ/mol; h_r = -1321 kJ/mol (exothermic)
Comp-C4	$C_{3.83}H_{7.5}N_{5.2}O_{5.23} \rightarrow 3.14\ H_2O + 2.60\ N_2 + 1.09\ CO_2 + 0.3\ CH_4 + 0.01\ H_2 + 2.43\ C$ Comp-C4 $\rightarrow$ 7.14 G + 2.44 C Mw_G = 25.5 g/mol; $h_{f,G}$ = -170 kJ/mol $h_{f,Comp\text{-}C4}$ = 16.0 kJ/mol; h_r = -1226 kJ/mol (exothermic)
PBX 9407	$C_{3.1}H_{5.9}N_{5.6}O_{5.6}Cl_{0.18}F_{0.18} \rightarrow 2.51\ H_2O + 2.82\ N_2 + 1.57\ CO_2 + 0.18$ HCL + 0.18 HF + 0.13 CH_4 + 1.40 C PBX 9407 $\rightarrow$ 7.37 G + 1.40 C Mw_G = 27.8 g/mol; $h_{f,G}$ = -176 kJ/mol $h_{f,PBX9407}$ = 18.4 kJ/mol; h_{rxn} = -1318 kJ/mol (exothermic)
PBXN-109	$C_{1.61}H_{2.94}N_{1.44}O_{1.51}AL_{0.62} \rightarrow 1.08\ H_2O + 0.72\ N_2 + 0.215\ CO_2 + 0.195\ CH_4 +$ 0.62 AL + 1.2 C (The aluminum is non-reactive in pre-ignition calculations) PBXN-109 $\rightarrow$ 2.21 G + 0.62 AL + 1.20 C Mw_G = 23.6 g/mol; $h_{f,G}$ = -163 kJ/mol $h_{f,PBXN109}$ = -4.7 kJ/mol; h_r = -355.6 kJ/mol (exothermic)
RDX	$C_3H_6N_6O_6 \rightarrow 2.7\ H_2O + 3\ N_2 + 1.65\ CO_2 + 0.15\ CH_4 + 1.2\ C$ RDX $\rightarrow$ 7.5 G + 1.2 C Mw_G = 27.7 g/mol; $h_{f,G}$ = -175 kJ/mol $h_{f,RDX}$ = 69 kJ/mol; h_r = -1382 kJ/mol (exothermic)
Semtex 1H	$C_{4.8}H_{8.86}N_{3.8}O_{6.51} \rightarrow 3.75\ H_2O + 1.9\ N_2 + 1.38\ CO_2 + 0.34\ CH_4 + 3.08\ C$ Semtex 1H $\rightarrow$ 7.37 G + 3.08 C Mw_G = 25.4 g/mol; $h_{f,G}$ = -200 kJ/mol $h_{f,Semtex\ 1H}$ = -226 kJ/mol; h_r = -1249 kJ/mol (exothermic)
XTX-8004	$C_{2.57}H_6N_{3.44}O_{3.86}Si_{0.43} \rightarrow 2.0\ H_2O + 1.72\ N_2 + 0.40\ CO_2 + 0.40\ CH_4 + 1.77\ C +$ 0.43 SiO_2 XTX-8004 $\rightarrow$ 4.72 G + 1.77 C + 0.43 SiO_2 Mw_G = 23.7 g/mol; $h_{f,G}$ = -152.4 kJ/mol, $h_{f,SiO4}$ = -911 kJ/mol $h_{f,XTX\text{-}8004}$ = -175.5 kJ/mol; h_r = -935.2 kJ/mol (exothermic)

X.1.5 *Micromechanics pressurization*. The conductive energy equation (Eq. 1) is coupled to a micromechanics pressurization (MMP) model through pressure (P) in Eq. (2). The MMP model is based on decomposition gases accumulating within a defect as shown in Fig. X.2. In Fig. 2, the initial defect is shown as a spherical cloud with various arrows describing how the defect changes inside until it ultimately fails.

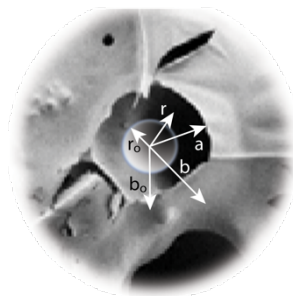

Figure X.2 Pore defect.

In Fig. 2, "r_o" represents the initial defect radius, "r" represents the radius of the pore after decomposition but prior to mechanical displacement, and "a" represents the pore radius after decomposition and includes mechanical displacement. The parameters b_o and b are related to the distance between two adjacent nucleation sites. The MMP model uses a simple damage criterion where the pore pressure is used to differentiate between open and closed pores. Gases can only migrate

between open pores and the headspace volume where pressure is typically measured. In contrast, gases within closed pores do not co-mingle.

The MMP model provides the local pressure by solving the displacement equations for a symmetric linear elastic material surrounding a pressurizing hollow sphere. The MMP parameters are listed in Table X.6 are required to determine the spatially dependent pressure. Derivation of the MMP model equations is beyond the scope of the current work but can be found in [7].

The MMP parameters for the RDX-based explosives include bulk modulus (K), Young's modulus (E), Poisson's ratio (ν), distance between nucleation sites (b_o = 0.000226 m), pore failure pressure (P_{fail} = 5×10^6 Pa), volumetric expansion coefficient (β) used to calculate thermal strain ($\tilde{\varepsilon}_T = \beta(T - T_o)$), and the volume fraction weighted mechanical strain, $\Delta\tilde{\varepsilon}_m$, which is caused by melting. Mechanical strain caused by polymorphic phase changes are assumed to be negligible. K, E, and ν were estimated from longitudinal (S_L) and shear (S_S) sound velocities. S_L and S_S were either obtained from [8, 9, 10, 11] or estimate using a linear correlation between crystal density (TMD) and sound speed. The volumetric coefficient of thermal expansion (β) was estimated using a linear correlation between K and β using data from the other explosives in [8].

The mechanical strain caused by melting for pure RDX, TNT, and PETN was determined with Eq. (6):

$$\Delta\tilde{\varepsilon}_m = \frac{\rho_{co}}{[1+\beta(T_m-300]\rho_L} - 1 \quad . \tag{6}$$

The mechanical strain is zero below the solidus temperature and $\Delta\tilde{\varepsilon}_m$ above the liquidus temperatures. This volume fraction weighted strain is transitioned using a cosine ramp function like shown in Eq. (4). For Comp-B, the additional mechanical strain associated with TNT is 0.048. For Semtex 1H, the additional mechanical strain associated with PETN is 0.031.

Table X.6 *MMP parameters.*

Name	ρ_{co} kg/m^3	S_L m/s	S_S m/s	K GPa	E GPa	ν	β 1/K	ϕ_{rdx}	$\phi_{rdx}\Delta\tilde{\varepsilon}_m$ RDX[b]
Comp-B3	1742	3.10	1.68	10.2	12.7	0.29	0.000164	0.579	0.038
Comp-C4	1659	3.26	1.84	10.2	14.2	0.27	0.000270	0.836	0.054
PBX 9407	1799	3.04	1.77	9.10	14.0	0.24	0.000198	0.937	0.061
PBXN-109	1656	0.38	0.053	0.233	0.014	0.49	0.000340	0.587	0.038
RDX	1806	3.52	2.08	12.0	19.3	0.23	0.000190	1.000	0.065
Semtex1H	1581	3.41	1.98	10.1	15.5	0.24	0.000370	0.376	0.024
XTX-8004	1579	3.41	1.98	3.4	3.2	0.34	0.000300	0.699	0.045

Additional MMP parameters include ρ_{co} which represents the crystal density (TMD) at room temperature (300 K) for pure RDX (1806 kg/m^3), TNT (1654 kg/m^3), and PETN (1778 kg/m^3). β represents volumetric expansion coefficient for pure RDX (0.00023 K^{-1}) [12], TNT (0.00016 K^{-1}) [12], and PETN (0.00025 K^{-1}) [12]. ρ_L represents liquid densities for RDX (1630 kg/m^3) [13], TNT (1472 kg/m^3) [14], and PETN (1600 kg/m^3, guessed). $\Delta\tilde{\varepsilon}_m$ is the mechanical strain due to melting for pure RDX (0.065), TNT (0.114), and PETN (0.080). The volume fraction of RDX is given in Table X.6. The volume fraction of TNT in Comp-B3 is 0.579. The volume fraction of PETN in Semtex 1H is 0.382.

X.2 SITI calibration/predictions

The Sandia Instrumented Thermal Ignition (SITI) experiment shown in Figure X.3(a) was used to determine the thermal conductivities listed in Table X.1 and the reaction parameters listed in in Table X.2 using measured temperatures at various radial positions. Calibration usually requires both a vented and sealed experiment. The remaining SITI experiments as well as the One-Dimensional Time-to-eXplosion (ODTX) experiments are used for validation. The ODTX experiment confines a 1.27 cm diameter sphere within constant temperature anvils as shown in Fig. X.3(b)

X.2.1 *SITI and ODTX configurations*. Typically, the SITI experiment confines two 2.54 cm diameter by 1.27 cm tall cylinders of HMX-based explosive in aluminum with nine type K 127 μm (0.005 in.) diameter thermocouples with measuring points located at radial positions in mm of 0, 1.70, 2.55, 3.40, 4.25, 5.11, 5.96, 8.81, and 11.7 and placed between the two explosive cylinders. The outer surface of the 7.62 cm diameter by 4.58 cm tall aluminum

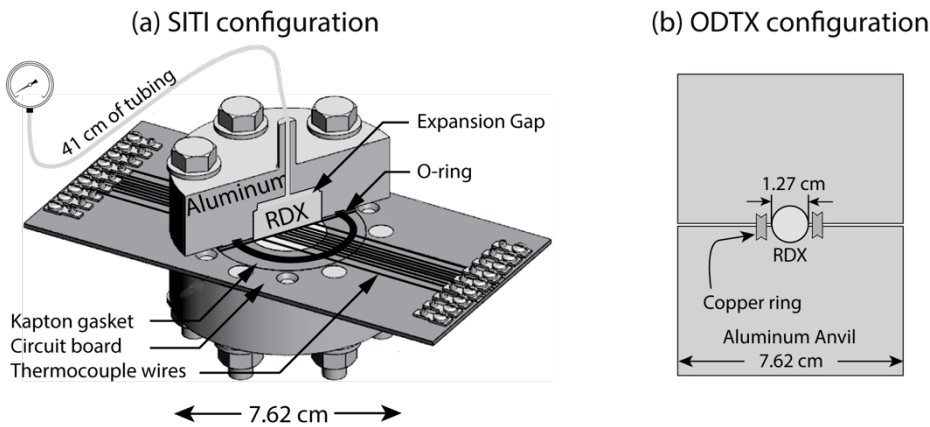

Figure X.3 (a) SITI and (b) ODTX configurations.

confinement is heated using rope heaters controlled by a thermocouple on the lateral surface. The external aluminum surface is heated to a set point temperature, T_{sp}, in 600 s and held until the explosive thermally ignites. Two expansion gaps that are above and below the explosive are also machined into the confining aluminum. Each expansion gap has a diameter of 2.22 cm and is 0.16 cm tall. The top expansion gap is connected to a calibrated Kulite Model HEM-375 pressure transducer.

ODTX experiments measure thermal ignition times in a 1.27 cm diameter sphere of explosive [15]. Two preheated 7.62 cm diameter by 5.08 cm high aluminum cylinders hydraulically confine a spherical sample to 150 MPa in a machined cavity with a knife edge channel surrounding the explosive. A copper gasket is used to retain the decomposition gases within the cavity. At time zero, preheated anvils are quickly placed around the explosive providing a constant temperature boundary temperature.

X.2.2. *Model and data comparisons*. The model was used to predict both internal temperature/pressure profiles as well as thermal ignition time for seven explosives as shown in Figs. X.4 and X.5. The plots on the left-hand side of these figures show a single individual SITI run from each explosive. The individual runs provide the measured/predicted temperature profiles at the nine thermocouple locations as well as the predicted pressure profiles at these radial locations. With the outer locations reaching high pressures prior to inner locations. The pressure profiles show a gradual increase followed by an abrupt decrease in pressure as the material is thermally damaged and transitions from a closed-pore structure to an open pore structure. Pressure in the open pore explosive is the same as in the expansion gap which is measured with the pressure transducer.

Figure X.4 and X.5 also provide the thermal ignition time for each of the seven explosives within the SITI configuration (middle plots) and the ODTX configuration (plots on right-hand side of the Figs. X.4 and X.5). Predicted ignition times for both the SITI experiments and the ODTX experiments show good agreement. A full uncertainty analysis for the RDX and PBXN-109 can be found in [16] indicating that the uncertainty is small in predicted ignition times even when input parameters are adjusted by $\pm 5\%$ of the mean values.

X.3 Summary and conclusions

The UCM/MMP model has been significantly simplified and used to model thermal ignition of seven explosives containing RDX: 1) Comp-B3, 2) Comp-C4, 3) PBX 9407, 4) PBXN-109, 5) RDX, 6) Semtex 1H, and (7) XTX-8004. The kinetic model consists of a single first order decomposition reaction using a pressure dependent distributed reaction rate based on the reaction extent. Pressure was determined as a field variable using a micromechanics pressurization model. The equilibrium product hierarchy was determined using the TIGER equilibrium code [6] with the product gas molecular weight

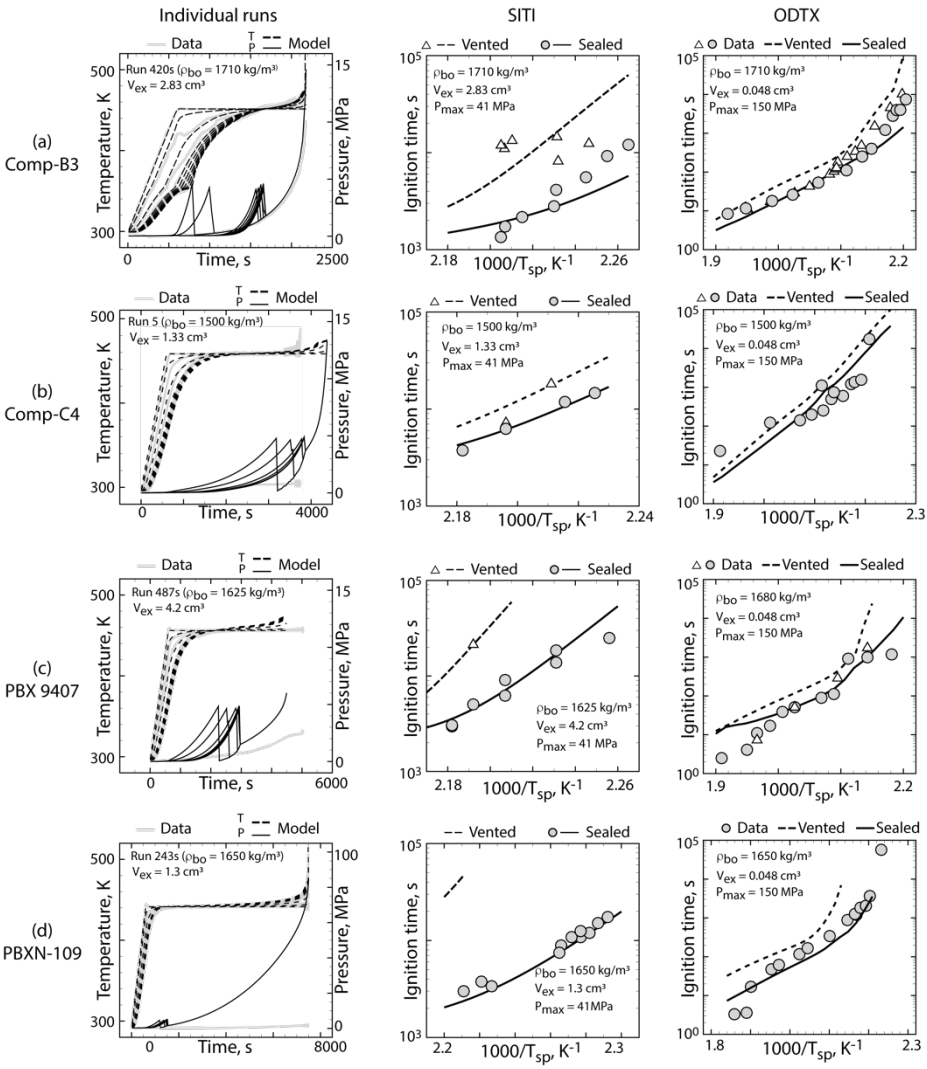

Figure X.4 Individual runs showing predicted and measured pressure, thermal ignition time for the SITI experiments, and thermal ignition times for the ODTX experiments for (a) Comp-B3, (b) Comp-C4, (c) PBX 9407, and (d) PBXN-109. More detail regarding the SITI data can be found in [1, 17, 18, 16]. Details regarding the ODTX data can be found in [1, 19, 20, 11].

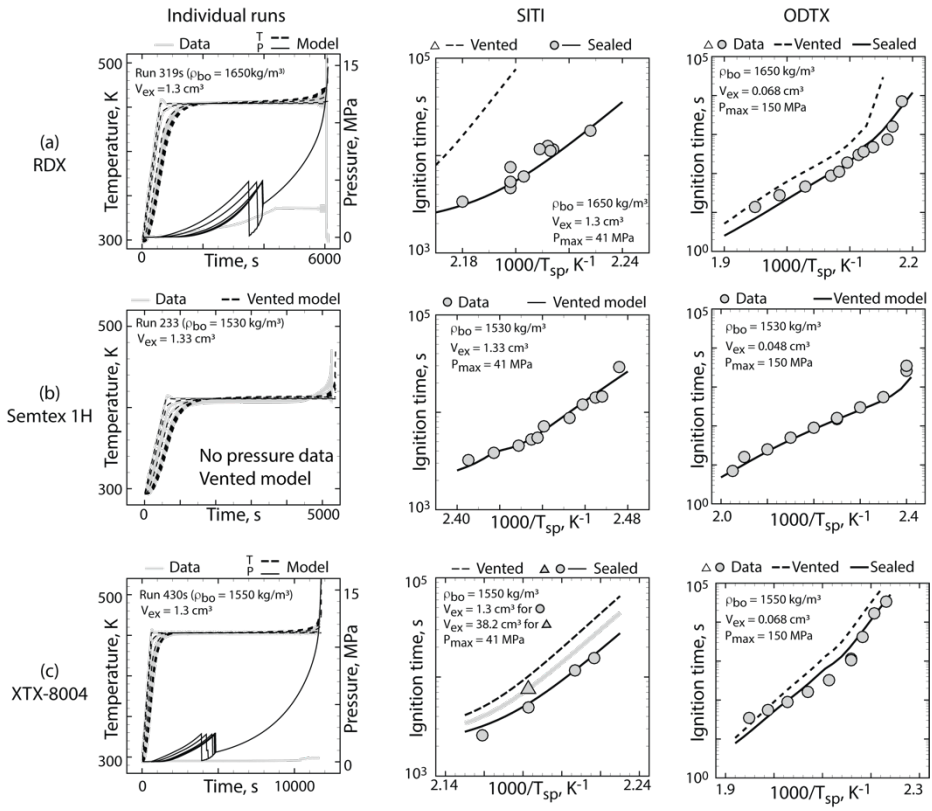

Figure X.5 Individual runs showing predicted and measured pressure, thermal ignition time for the SITI experiments, and thermal ignition times for the ODTX experiments for (a) RDX, (b) Semtex 1H, and (c) XTX-8004. More detail regarding the RDX SITI data can be found in [21]. Details regarding the ODTX data can be found in [19, 22, 23].

and heat of formation determined using a mole fraction based mixing rule. The model was calibrated with both vented and sealed SITI experiments and validated with additional SITI experiments as well as ODTX experiments.

The SITI data was taken between 2004-2017: 1) 2013 for Comp-B, 2) 2007 Comp-C4, 3) 2016 for PBX 9407, 4) 2002 for PBXN-109, 5) 2004 for RDX,6) 2004 for Semtex, and 7) 2015 for XTX-8004. Although we attempted to measure pressure in these experiments, we were not always successful. Primary problems included plugging of the pressure tubing which prevented data acquisition for the sealed tests. Plugging of the vent port may have also caused data interpretation errors for the vented tests. The best measurements were for the Comp-B experiments. In fact, no pressure measurements were obtained for the Semtex 1H experiments and the pressure exponent was set to zero. Pressure measurements were also inadequate for PBXN-109 and the pressure exponent was assumed to be the same as for the RDX model.

Although the model adequately matched all the older cookoff data, there is a need for better small-scale cookoff experiments that are well characterized and include internal temperature as well as pressure. Such experiments should include details regarding any headspace that could fill with decomposition gases. Care should be taken to prevent restriction of the pressure tubing. Experiments should consider investigating cookoff in low density, even shredded, explosives to prevent holdup of gases within the interior of the explosives. Higher density experiments that match the intended applications can be used for model validation and for further safety calculations.

ACKNOWLEDGEMENTS

We would also like to thank Shane Snedigar for running the SITI experiments, Farhan Rahman and John Tencer for internal review, and Jeremy Lechman for management support.

Sandia National Laboratories is a multi-mission laboratory managed and operated by National Technology & Engineering Solutions of Sandia, LLC (NTESS), a wholly owned subsidiary of Honeywell International Inc., for the U.S. Department of Energy's National Nuclear Security Administration (DOE/NNSA) under contract DE-NA0003525. This written work is authored by an employee of NTESS. The employee, not NTESS, owns the right, title, and interest in and to the written work and is responsible for its contents. Any subjective views or opinions that might be expressed in the written work do not necessarily represent the views of the U.S. Government. The publisher acknowledges that the U.S. Government retains a non-exclusive, paid-up, irrevocable, world-wide license to publish or reproduce the published form of this written work or allow others to do so, for U.S. Government purposes. The DOE will provide access to results of federally sponsored research in accordance with the DOE Public Access Plan.

X REFERENCES

[1] M. L. Hobbs, M. J. Kaneshige, W. W. Erikson, J. A. Brown, M. U. Anderson, S. N. Todd and D. G. Moore, "Modeling of a Melt Cast Explosive (Comp-B)," *Combust. Flame,* vol. 215, pp. 36-50, 2020.

[2] Z. D. Lawless, M. L. Hobbs and M. J. Kaneshige, "Thermal conductivity of energetic materials," *Journal of Energetic Materials,* vol. 38, no. 2, pp. 214-239, 2020.

[3] M. L. Hobbs, M. J. Kaneshige and W. W. Erikson, "A UNIVERSAL COOKOFF MODEL FOR EXPLOSIVES," in *50th International Annual Conference of the Fraunhofer ICT*, Karlsruhe, 2019.

[4] M. L. Hobbs, M. J. Kaneshige, S. N. Todd and T. R. Krawietz, "RDX solubility in TNT at high temperatures," *J. Therm. Anal. Calorim.,* vol. 142, pp. 861-869, 2020.

[5] M. L. Hobbs and M. J. Kaneshige, "Transforming polymorphs, melting, and boiling during cookoff of PETN," *Combust. Flame,* vol. 237, p. https://doi.org/10.1016/j.combustflame.2021.111877, 2022.

[6] M. L. Hobbs, R. G. Schmitt, H. K. Moffat and Z. Lawless, "JCZS3--an improved database for EOS calculations," in *16th International Detonation Symposium*, Cambridge, 2018.

[7] M. L. Hobbs, J. A. Brown, M. J. Kaneshige and C. Aviles-Ramos, "Micromechanics Pressurization Model for Cookoff," *Propellants, Explosives, Pyrotechnics,* vol. 47, p. DOI: 10.1002/202100155, 2022.

[8] S. P. Marsh, LASL Shock Hugoniot Data, Berkeley: University of California Press, 1980.

[9] B. M. Dobratz and P. C. Crawford, "LLNL Explosives Handbook Properties of Chemical Explosives and Explosive Simulants," Lawrence Livermore National Laboratory , Livermore, 1985.

[10] J. J. Haycraft, L. L. Stevens and C. J. Eckhardt, "The elastic constants and related properties of the energetic material cyclotrimethylene trinitramine (RDX) determined by Brillouin scattering," *J. Chem. Phys.,* vol. 124, p. 024712, 2006.

[11] M. A. McClelland, T. D. Tran, B. J. Cunningham, R. K. Weese and J. L. Maienschein, "Cookoff response of PBXN-109: material characterization and ALE3D thermal predictions," in *Insensitive Munitions & Energetic Materials technology Symposium*, Saint-Malo, 2003.

[12] T. R. Gibbs and A. Popolato, LASL Explosive Property Data, Berkeley: Ccalifornia Press, 1980.

[13] D. W. Carlson, G. W. Nauflett, J. W. Brasch and T. D. Austin, "Thermodynamic and melting properties of RDX at elevated pressure," in *17th JANNAF Combustion Meeting*, Hampton, 1980.

[14] D. M. Dattelbaum, R. S. Chellappa, P. R. Bowden, J. D. Coe and M. A. Margevicius, "Chemical stability of molten 2,4,6-trinitrotoluene at high pressure," *Appl. Phys. Lett.,* vol. 104, p. 021911, 2014.

[15] P. C. Hsu, G. Hust, C. May, M. Howard, S. K. Chidester, H. K. Springer and J. L. Maienschein, "Study of thermal sensitivity and thermal explosion violence of energetic materials in the LLNL ODTX system," *AIP Conf. Proc.,* vol. 1426, pp. 559-562, 2012.

[16] M. L. Hobbs, M. J. Kaneshige and W. W. Erikson, "A UCM/MMP cookoff model of PBXN-109 and RDX," in *JANNAF 34th ESHS Joint Meeting*, Salt Lake City, 2023.

[17] M. L. Hobbs, M. J. Kaneshige, W. W. Erikson, J. A. Brown, M. U. Anderson, S. N. Todd and D. G. Moore, "Cookoff experiments of a melt cast explosive (Comp-B3)," *Combust. Flame,* vol. 213, pp. 268-278, 2020.

[18] M. L. Hobbs, M. J. Kaneshige and C. D. Yarrington, "Large deformation and gas retention during cookoff of a plastic bonded explosive (PBX 9407)," *Combust. Flame,* vol. 198, pp. 278-289, 2018.

[19] P. C. Hsu, G. Hust, W. M. Howard and J. L. Maienschein, "The ODTX system for thermal ignition and thermal safety study of energetic materials," in *Fourteenth International Detonation Symposium*, Coeur d'Alene, 2010.

[20] P. C. Hsu, S. Strout, M. McClelland and F. Ellsworth, "One-dimensional time to explosion (thermal sensitivity) tests on PETN, PBX-9407, LX-10, and LX-17," Lawrence Livermore National Laboratory Report LLNL-TR-681467, Livermore, 2016.

[21] M. L. Hobbs, M. Steyskal and M. J. Kaneshige, "Modeling RDX Ignition," in *JANNAF 24th Propulsion Systems Hazards Subcommittee Meeting*, Newton, 2008.

[22] R. R. McGuire and C. M. Tarver, "Chemical decomposition models for the thermal explosion of confined HMX, TATB, RDX, and TNT explosives," in *7th International Symposium on Detonation*, Annapolis, 1981.

[23] P. C. Hsu, S. Strout, A. Nye and R. Ganeriwala, "Thermal safety characterization of HMX, LX-07, PBX 9502, and XTX-8004 (Lot C-639) in the ODTX system," Lawrence Livermore National Laboratory, LLNL-TR-771282, Livermore, 2019.